Peer-reviewed version available at Atmosphere 2018, 9, 352; doi:10.3390/atmos9090352

Article

Effects of El-Niño, Indian Ocean Dipole and Madden-Julian Oscillation on Sea Surface Temperature and Rainfall Anomalies in Southeast Asia. Case Study: Biomass Burning Episode of 2015

Amirul Islam [1,*], Andy Chan [1,*], Matthew Ashfold[2], Chel Gee Ooi [3], Majid Azari[1]

1. Department of Civil Engineering, Faculty of Engineering, University of Nottingham, Malaysia Campus, Jalan Broga, 43500, Semenyih, Selangor, Malaysia; andy.chan@nottingham.edu.my
2. School of Environmental and Geographical Sciences, Faculty of Science, University of Nottingham, Malaysia Campus, Jalan Broga, 43500, Semenyih, Selangor, Malaysia; matthew.ashfold@nottingham.edu.my
3. Department of Atmospheric Sciences, National Central University, 32001, Chung-Li, Taiwan, ROC; chelgee.ooi@gmail.com

*Correspondence: islamccs@gmail.com ; Tel: +60-11-24339597 and andy.chan@nottingham.edu.my; Tel: +60-12-3859922

Abstract: Maritime Continent (MC) positions in between Asian and Australian summer monsoons zone. Its complex topography and shallow seas around it is a major challenge for the climate researchers to model and understand it. Monsoon in this area is affected by inter-scale ocean-atmospheric interactions like El-Niño Southern Oscillation (ENSO), Indian Ocean Dipole (IOD) and Madden-Julian Oscillation. Monsoon rainfall in MC (especially in Indonesia and Malaysia) profoundly exhibits its variability dependency on ocean-atmospheric phenomena in this region. This monsoon shift often introduces to dreadful events like biomass burning (BB) in Southeast Asia (SEA) which sometimes leads to severe trans-boundary haze pollution. In this study, the episode of BB in 2015 of SEA is highlighted and discussed. Observational satellite datasets are tested by performing simulations with numerical weather prediction (NWP) model using WRF-ARW (Advanced research WRF). Observed and model datasets are compared to study the sea surface temperature (SST) and precipitation (rainfall) anomalies influenced by ENSO, IOD and MJO. Correlations have been recognised which explains the delayed rainfall of regular monsoon in MC due to the influence of ENSO, IOD and MJO during 2015 BB episode, eventually leading to intensification of fire and severe haze.

Keywords: monsoon, maritime continent, ocean-atmospheric phenomena, Southeast Asia, biomass burning, sea surface temperature, rainfall.

1. Introduction

In climate research, the maritime continent (MC) is one of the most crucial regions to study [1]. MC can play a key role as heat and moisture source and can impact global atmospheric circulations and contribute to climate change [2]. MC is known to be the most active convective region where convection is influenced by local, regional and global atmospheric conditions such as monsoon, tropical convection, intra-seasonal oscillations and complex structure of the topography of land and sea around it [3,4]. The intertropical convergence zone (ITCZ) and its correlations with sea surface temperature (SST) and active precipitation are mostly responsible for convection in the MC region [5]. Despite its importance, inter-scale interactions of intra-seasonal and mesoscale variability forced by diurnal affects (e.g. oceanic circulation, wind, temperature and precipitation) errors are often found in the climate models of MC [6]. The MC has a signature seasonal cycle in its rainfall characterizing a typical monsoon climate [7]. Due to intricate topography of the region and vast unpopulated land areas dense rain gauge network is absent in most of the places of MC and gauge observation in the oceanic areas are also not became possible to obtain so far [8]. Satellite observation is the best available solution in such case to attain adequate temporal and spatial coverage of rainfall data [9]. Therefore, in this study computer model is used using the satellite data to investigate SST and rainfall. In the southern equator principally, rainy season peaks in DJF (December-February) and the drier season peaks in July-August [10].

Peer-reviewed version available at Atmosphere 2018, 9, 352; doi:10.3390/atmos9090352

In the atmosphere, the most important source of pollution is fire which comes in forms of aerosol particles, greenhouse gases and different trace gases [11]. Not only the air quality is depended on fire, but also the whole ecosystem, public health, land use and safety. Improvements of satellite data provide better observational skills to study weather and climate more comprehensively. Global emission inventories are checked regularly near real time. Spatial resolution of satellite imageries has been improved which now helps to obtain data on hourly basis [12].

BB in SEA is a regular event and generates air pollution on a very large scale (while propagates as haze) with immense impacts on economics and public health that spreads over the MC [13]. BB events usually occur in dry seasons and vary in degrees. Since 1972, almost all hazes in SEA region have been recorded as trans-boundary [14]. Slash-and-burn practice mostly in Indonesia and illegal extension of agricultural lands are the main anthropogenic reasons of BB in MC region. Historically it starts from Southern Sumatra and Kalimantan on Indonesian part of Borneo [15]. In early 2000s, after the Earth Observing Satellite System by NASA started its observations it has shown that 2015 BB and its haze episode in SEA was the most severe in terms of fire activity and pollution and CO_2 equivalent BB emission during 2015 episode alone stood for 2013 annual CO_2 emissions of Japan and India combined [16]. Dry condition is mainly responsible for such events. BB has its direct impacts on weather, climate and public health [17]. In recent years, the MC has experienced multiple numbers of major trans-boundary haze episodes (from 1982 until 2015). Ground observation stations, satellites and records of airport visibility system in Sumatra and Kalimantan region (Indonesia) demonstrated that after 1994 and 1997 BB episodes the 2015 episode ranked among the worst on record [17]. The increasing numbers of BB episodes in the MC caused extra economic damages. BBs and the evolved haze propagate across national boundaries and contributes to the climate change in the entire MC.

Haze episodes in MC initially start because of peatland fires in Indonesia and appeared to be influenced greatly by several major ocean-atmosphere events e.g. ENSO, IOD and MJO. The most important climatic element of MC is its rainfall [18]. MC is situated in Asian-Australian monsoon region and specialty of this region is annual wet and dry season cycle [19]. Over Indonesia the variability in rainfall is strongly related to ENSO and the rainfall is anomalously low during the warm period when El-Niño is existing [20]. This relationship is usually stronger during dry and transition seasons. Indian Ocean Dipole (IOD) is another significant ocean-atmospheric event that is responsible for rainfall anomalies in the MC region. IOD and ENSO caused rainfall variability is unique in the Indonesian region. Strong influence is observed during drier season (June-November) and in wet season (December-May) it is weaker [21]. Intra-seasonal variability in the MC is caused by another ocean-atmosphere phenomenon - MJO and it is associated with enhanced or suppressed convection and cloudiness which with a period of 30-90 days on average propagates from the Indian Ocean towards the Pacific Ocean [22]. Although MJO is usually observed to be weakening as it reaches the MC, but it is also observed sometimes when MJO initiates in the Indian Ocean but do not propagate through MC [23]. Asian-Australian monsoon covers the MC and northern part of Australia and creates annual dry and wet season [13] and MJO that passes through this region is associated with either high or extremely low precipitation [23].

Transboundary haze episodes of Malaysia and Indonesia introduced the local climate to catastrophic air pollution events which contributed to the climatic change of the whole SEA. However, the rational sequences of such behavior are yet unclear as these BB events are not still well understood by any established theories or quantified properly by measured data. Therefore, it is important to establish logical sequences, physically and prognostically, to understand why and how this is happening to learn how to take necessary steps earlier to avoid and combat them. BB episode of 2015 earned its global attention due to its big scale coverage and trans-boundary haze propagation and in details it is not well studied by the climate experts so far.

This study is focused especially on 2015 BB episode of SEA and to investigate the possibilities of influences of ocean-atmosphere events (MJO, ENSO and IOD) on the intensification of the episode. We attempt to find the correlation of monsoon with seasonal and intra-seasonal oscillations. The IOD and ENSO correlations with their single and concurrent effects and MJO effects on precipitation (rainfall) are investigated and the outcomes are discussed.

Preprints (www.preprints.org) | NOT PEER-REVIEWED | Posted: 19 June 2018 doi:10.20944/preprints201806.0304.v1

Peer-reviewed version available at Atmosphere 2018, 9, 352; doi:10.3390/atmos9090352

2. Data and methods

2.1 Data

Irregular periodic variation in SST and winds over the tropical eastern Pacific Ocean that affects the climate of tropics and subtropics is ENSO. Multivariate ENSO Index (MEI) is a parameter used to measure the intensity of ENSO in different months of the year and thus characterises it. For monitoring ENSO on a regular basis, the most comprehensive index is MEI as it can combine the analysis of both meteorological and oceanic components [24]. MEI is determined by International Comprehensive Ocean-Atmosphere Data Set (ICOADS). MEI datasets are used in this study and collected from the regularly updated archive of Earth System Research Laboratory (ESRL) of National Oceanic and Atmospheric Administration (NOAA) [25].

Another irregular oscillation of SSTs where the western Indian Ocean becomes alternately warmer and then colder than the eastern part of the ocean is characterised by IOD. The intensity of IOD is represented by Dipole Mode Index (DMI) which shows SST gradient between western equatorial Indian Ocean (50E-70E and 10S-10N) and south eastern equatorial Indian Ocean (90E-110E and 10S-0N) [27]. DMI datasets are used in this study and collected from the Global Climate Observing System (GCOS) datasets archive which is a funded program under World Meteorological Organization (WMO) [26].

In the tropical atmosphere the largest element of intra-seasonal variability (30-90 days) is MJO which is characterized by eastward progression of both enhanced and suppressed tropical rainfall and observed mainly over Indian and Pacific Ocean. Wheeler and Hendon [28] proposed an index that is seasonally independent to describe and monitor MJO properly. The index is based on a pair of empirical orthogonal functions (EOFs) that give an effective series to monitor MJO in real time called Real-Time Multivariate MJO series (RMM1 and RMM2). MJO phase progressions are generally illustrated by a phase diagram. RMM1 and RMM2 are mathematical models that combine cloud amount and winds thus provide a measure of MJO intensity in real time and location of its existence. MJO indices move anti-clockwise and from west to east. When index is located inside the circle at the centre (Figure A3) MJO is considered weakest, whereas outside the circle and as far it goes out of the circle it becomes stronger. MJO diagram has eight different phases to identify its location and progression in real time with least errors. Bureau of Meteorology, Australia regularly measures and updates MJO phases, their intensity and location [29].

Outgoing longwave radiation (OLR) is also considered for the study which is the electromagnetic radiation emitted from Earth and its atmosphere in the form of thermal radiation and measured in W/m^2 [30]. OLR shows map associated with cloudiness (normal, below normal and above normal) and allows to identify cloudiness over a specific region. Bureau of Meteorology, Australia regularly updates the OLR maps too and data for the study are collected from the archive [31].

Satellite datasets [32] show that all the year-round biomasses are continuously burning (more or less) either because of natural or anthropogenic reasons. But BB in the MC expands uncontrollably during the drier season (June-November) [16]. Rainfall can mitigate BB events to prevent them to form as disastrous as during 2015 BB episode in SEA. For this study we collect and study monthly rainfall analysis data of MC (July-December 2015) [33].

WRF-ARW (Advanced Research WRF) version 3.7 is used as weather simulation tool for this study. WRF is a numerical weather prediction (NWP) system that is designed for simulating satellite data and predict the atmosphere by computer models. It contains different ranges of meteorological applications where the scales range from meters to thousands of kilometers. Global Data Assimilation Systems (GDAS) continuously gathers observational data from the Global Telecommunications System (GTS) and other verified sources. The GDAS product used for this study is 'NCEP/GDAS FNL 0.25-degree Global Tropospheric Analyses and Forecast Grids' [34].

2.2 Method

In this study, we investigate the 2015 period which was El-Niño all the year round [35]. In order to understand the significance of 2015 MEI, values of two consecutive years (before and after 2015) have been observed and compared including 2013, 2014, 2016 and 2017.

Positive values of DMI indicate positive IOD and negative values indicate negative IOD. Similarly, as MEI, five years of data (2013-2017) have been observed and compared. Comparative evaluation confirmed much higher than normal DMI value during 2015 BB episode and its consequences are discussed.

MJO datasets provide visual data which show MJO intensity and their location in a given date. As MJO is a 30-90 days intra-seasonal variability, therefore 3 months of data in 2 stages (July-September and October-December) have been observed for five years (2013-2017) to identify the significance of MJO during 2015 BB period (July-October). Enhanced and suppressed rainfall influenced by MJO intensity and the effects on the MC region are discussed.

OLR is used to identify tall, thick and convective clouds and rain. Four years (2014-2017) of visual OLR data have been observed and analyzed with respect to the MJO phase data of same years.

All these datasets are analysed with respect to ENSO, IOD, MJO and OLR datasets for 2015 (July-December). Observation and analysis confirmed correlations and outcomes are discussed.

GRIB (Gridded Binary) data for 4 months (July-October 2015) are simulated for the computer model. The model concentrated on 2 variables - sea surface temperature (SST) and precipitation rate. Simulated wrfoutput files (netCDF) are postprocessed by ArcGIS (ArcMap version 10.2.2) to view simulated images for postprocess analysis. Physics and their schemes that are used for the WRF-ARW model are shown in Table A1.

The postprocessed WRF model and ground observation data are compared to calculate RMSE (root mean squared error) for both variables (SST and precipitation (rainfall) (see Table A2 - a and b).

Using the following equations (1) and (2) MSE and RMSE have been calculated respectively:

$$MSE = \frac{\sum_{i=1}^{n}(O_i - M_i)^2}{n} \quad (1)$$

$$RMSE = \sqrt{\frac{\sum_{i=1}^{n}(O_i - M_i)^2}{n}} \quad (2)$$

where,
MSE – mean squared error
RMSE – root mean squared error
i - number of value (e.g. 1,2,3, …)
n - total number of values
O - observed value
M - model value

3. Result analysis and discussions

3.1 Concurrent ENSO and positive IOD in 2015

Ocean-atmosphere interactions result ENSO in the Pacific Ocean and IOD in the Indian Ocean. Both phenomena can be generally identified by SST anomaly and the impact can be seen on precipitation in the MC and around the world. Ashok and Guan [36] identified the effects of single ENSO or IOD and their concurrent movement on Indian summer monsoon. IOD influences the rainfall significantly and reduces the impact of ENSO while merging alongside. BB episode of 2015 started in late July and lasted until late October. Therefore, MEI and DMI values are observed from July to October and also 2013-2017 data are analysed to understand how different 2015 was comparatively with the other years. Figure A2(a) and Figure A2(b) illustrate that in 2015 both MEI and DMI values were much higher comparatively with the other years and they concurred during 2015 BB episode. Meyers et. al [37] reported that positive IOD and El-Niño together causes decreasing rainfall and therefore during 2015 BB episode the MC region saw below average precipitation. Concurrence of La-Niña and negative IOD causes the opposite effect which increases rainfall in the region.

3.2 MJO, OLR and suppressed rainfall during 2015 BB episode

MJO initially originates over the Indian Ocean and propagates toward east at a speed of 5 ms^{-1} through the tropical belt. It later passes through MC region and finally decaying over the date line in the Pacific Ocean [38]. Stronger and weaker MJO correspond to enhanced (convective) and suppressed rainfall respectively in the channel MJO passes through.

In Figure A3, MJO phases of 2013-2017 (July-December) are illustrated to compare 2015 MJO phases with other years before and after it. BB episode of 2015 in SEA started in late July and continued until mid-October [13]. Figure A3 (e) shows MJO phase during JAS (July-September) and illustrates that the phase was strong at the beginning of July, but by the end of July the phase was located inside the circle which means the MJO intensity became very weak (suppressed rainfall state) and it continued until the end of September although the MJO was passing through the MC only after mid-September. Figure A3 (f) shows MJO phases for OND (October-December) where it is seen that after mid-October the MJO phases started getting stronger (enhanced rainfall state) while passing through the Indian Ocean and moving towards MC (easterly direction). Only in December MJO phase was passing through the MC with strong intensity. By the end of December, the MJO phase ended up in the western Pacific Ocean.

Figure A4 (a) illustrates global outgoing longwave radiation (OLR) from August to October which highlights regions experiencing more or less cloudiness [31]. The circled mark in Figure A4 (a) indicates our area of interest - the MC. To study 2015 BB episode, OLR data for other years (2014, 2016 and 2017) also are compared with 2015 OLR datasets. Figure A4 (a) clearly shows that the cloudiness during BB period in 2015 is much lower comparatively with other years before and after it. This correlation of OLR with MJO of the same period (discussed above) confirms the drier than normal season in MC.

Monthly rainfall analysis data (mm/month) of MC [33] in Figure A4 (b) is another correlation of rainfall anomaly with respect to MJO and OLR datasets of 2015 BB episode. Rainfall anomaly of July-December is illustrated in Figure A4 (b) where it is seen that rainfall over Sumatra and Kalimantan were far below average during the peak of BB episode of 2015 (August-October) when the MJO intensity was very weak and OLR also much lower than the average. In November and December, the normal rainfall came back to the MC when MJO intensity became stronger as illustrated in Figure A3 (f) and OLR also became above average [29].

3.3 Model data (SST and precipitation) analysis from MEI, DMI, MJO and OLR viewpoint

Using NWP model WRF-ARW the following Figure A5 (for SST) and Figure A6 (for precipitation) are simulated.

From Figure A5 it is seen that throughout the entire 2015 BB episode starting from July until October SST was increasing gradually from 304.496 K (31.346 °C) (highest in July 2015) up to 310.4 K (37.25 °C) (highest in October 2015) with RMSE ≈ 2.43. This has a good correlation with MJO and OLR data (higher temperature causes drier condition) that caused suppressed rainfall in the BB effected region. Intra-seasonal variance of OLR almost triples between 26°C and 35°C [39] and during the 2015 BB episode the average temperature (AUG-OCT) derived from Table A2 (a) was 303.63 K (30.48°C). Figure A5 also shows lower land temperature in the hilly areas in Malaysia, shoresides in western Sumatra and dense forest areas in central Kalimantan.

Figure A2 (a) and A2 (b) explain that in 2015 El-Niño and positive phase of IOD merged concurrently. El-Niño kept intensified from the beginning of the year with MEI value from July until September ($1.987 < 2.365 < 2.532$) and then slightly dropped later in October to 2.256. During the same time DMI value raised from 0.674 to 0.853. It supports the statement that positive IOD reduces the impact of ENSO while merging concurrently [36].

Figure A3 (e) shows how in the beginning of July 2015 MJO started moving from western Pacific with a strong intensity. By the time it approached western hemisphere and Africa and was passing through it the intensity started becoming weaker and by the end of July as it was approaching Indian Ocean it became very weak. This weak phase of MJO continued until the end of September and by the end of September the MJO was located at the center of the circle which means the MJO then was at its weakest possible state. This time MJO was passing across Indonesia through MC. This state of MJO phase created much drier than average season in MC which ended up with rainfall much lower than average (less than 3 mm) as Table A2(b) shows. During this period BB of 2015 was at its peak. This condition is also approved by the OLR diagram from

Figure A4(a) of 2015 and the visual rainfall data of months July, August and September in Figure A4(b). Again, Figure A3(f) shows the MJO phase diagram of months October, November and December 2015 where the MJO intensity kept becoming stronger until mid-November. Later in November became a little weaker and then kept intensifying until the end of December through the MC which brought enhanced convection in MC and therefore more rainfall (Figure A4(b) – October-December) which mitigated the BB of 2015 episode.

4. Conclusion

The study asserts that the biomass burning episode of 2015 in Southeast Asia was strongly influenced by concurrence of ENSO and positive IOD phenomenon which increased the SST and made the MC surroundings a hot bed for increased burning. The outgoing longwave radiation and MJO during the episode confirms the suppressed convection during the episode and model data illustrated extremely low (much below the normal) precipitation. All these mean that the BB episodes are intensified by coincidental climatic phenomena.

A number of studies still need to be conducted to have more detailed information. The mechanisms of El-Niño and positive IOD formation particularly for the 2015 episode still need to be studied. We need better understanding about non-uniform rainfall response during El-Niño in boreal winter and boreal summer. Whether direct linear or non-linear correlations exist among ENSO, IOD and MJO or not is also a big question. How the vast haze formed due to the BB in 2015, propagated through the MC and how it impacted the regional climate also needs to be investigated.

Author contributions: Amirul Islam designed and performed simulation and wrote the paper. Chel Gee Ooi co-designed and provided critical revision. Majid Azari contributed to ground observation data collection and analyzing the data. Matthew Ashfold contributed to the conception, design of the study and provided critical revision. Andy Chan ensured the accuracy of the article, provided critical revision of the article and provided final approval of the version to be submitted to publish.

Acknowledgments: The study is supported by Malaysian Ministry of Science, Technology and Innovation (MOSTI) under project: "Biomass burning haze (BBH) in Southeast Asia (SEA): Development of a computational tool to predict its transport and impacts on climate change in Malaysia (Nottingham00009)". The model computations were run on the cluster supported by High Performance Computing (HPC) facility of University of Nottingham, UK campus.

Conflicts of interest: The authors declare no conflict of interest.

Preprints (www.preprints.org) | NOT PEER-REVIEWED | Posted: 19 June 2018 doi:10.20944/preprints201806.0304.v1

Peer-reviewed version available at Atmosphere 2018, 9, 352; doi:10.3390/atmos9090352

Appendix

Table A1: Physics and schemes used for the WRF-ARW model

Physics (processes)	Schemes description
Microphysics scheme	WRF single-Moment (WSM) 3-class [40]
Long-wave radiation scheme	RRTM (Rapid Radiative Transfer Model) scheme [41]
Short-wave radiation scheme	Dudhia scheme [42]
Surface layer scheme	Monin-Obukhov similarity scheme [43]
Land surface model	Noah-MP Land Surface model [44]
Planetary boundary layer (PBL) scheme	Yonsei University scheme (YSU) [45]
Cumulus parameterisation scheme	Kain-Fritsch (new Eta) scheme [46]

Table A2: RMSE calculation for SST, K (a) and precipitation, mm (b)

2015 (SST) K	**Observed value (mean) O_i**	**Model value (mean) M_i**	**Absolute Error $\lvert(O_i - M_i)\rvert$**	**Square of Absolute Error $\lvert(O_i - M_i)\rvert^2$**	**MSE**	**RMSE**
Months						
JUL	303.48	300.9	2.5	6.25		
AUG	303.65	301.2	2.5	6.07	5.9	≈2.43
SEP	303.38	300.9	2.5	6.18		
OCT	303.85	301.6	2.3	5.19		

(a)

2015 (precipitation) mm	**Observed value (mean) O_i**	**Model value (mean) M_i**	**Absolute Error $\lvert(O_i - M_i)\rvert$**	**Square of Absolute Error $\lvert(O_i - M_i)\rvert^2$**	**MSE**	**RMSE**
Months						
JUL	1.74	1.15	0.59	0.35		
AUG	1.38	1.17	0.21	0.04	0.24	≈0.49
SEP	1.90	1.30	0.63	0.40		
OCT	2.63	2.25	0.38	0.15		

(b)

Table A2 - (a) and (b) describe the MSE and RMSE calculation process step by step. The calculated values of RMSE for SST and precipitation are 2.43 and 0.49 respectively.

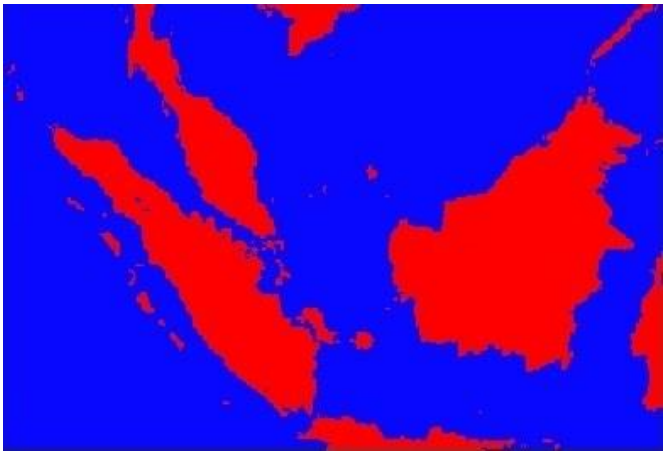

Figure A1: Selected zone of our study and for running the NWP model with WRF-ARW. Figure shows the land (red) and sea area (blue) of Malaysia and Indonesia (Sumatra and Kalimantan) - main region where in SEA the BB episode occurred in 2015.

Peer-reviewed version available at Atmosphere 2018, 9, 352; doi:10.3390/atmos9090352

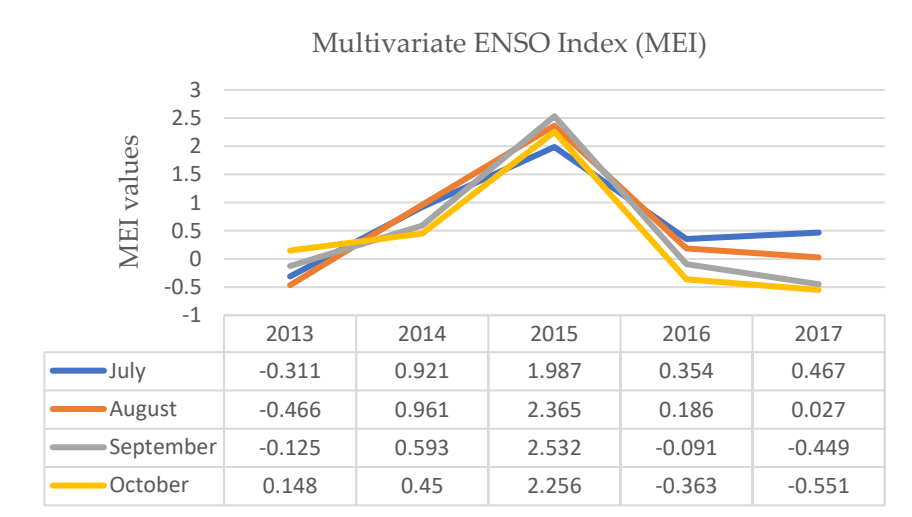

	2013	2014	2015	2016	2017
July	-0.311	0.921	1.987	0.354	0.467
August	-0.466	0.961	2.365	0.186	0.027
September	-0.125	0.593	2.532	-0.091	-0.449
October	0.148	0.45	2.256	-0.363	-0.551

Figure A2 (a): Multivariate ENSO Index (MEI) data [35] show the values in July, August, September and October (2013-2017). The graph shows that the highest MEI values were in 2015. In September 2015 MEI value was highest when the BB of 2015 episode was in its peak.

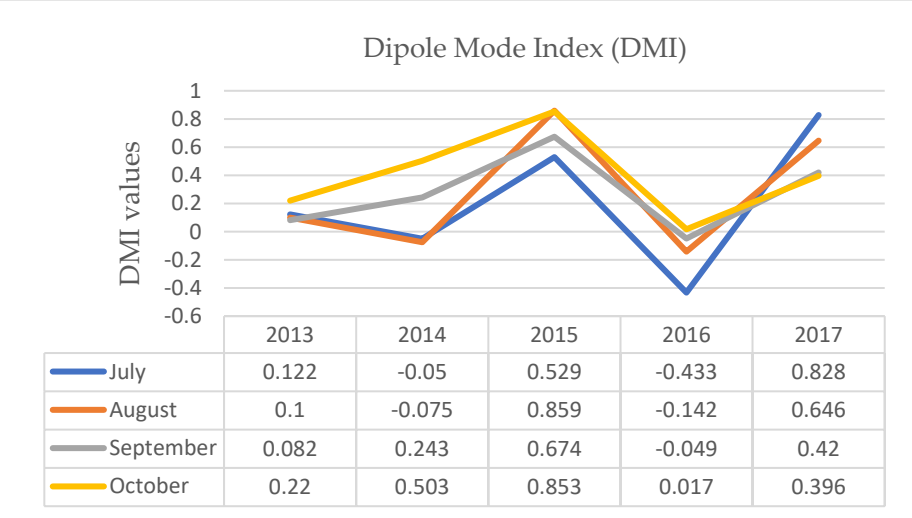

	2013	2014	2015	2016	2017
July	0.122	-0.05	0.529	-0.433	0.828
August	0.1	-0.075	0.859	-0.142	0.646
September	0.082	0.243	0.674	-0.049	0.42
October	0.22	0.503	0.853	0.017	0.396

Figure A2 (b): Dipole Mode Index (DMI) [47] values are shown in the graphs from 2013 until 2017. Positive IOD with higher DMI values in 2015 concurrently with higher MEI during the same period intensified the BB episode.

 doi:10.20944/preprints201806.0304.v1

Peer-reviewed version available at *Atmosphere* **2018**, *9*, 352; doi:10.3390/atmos9090352

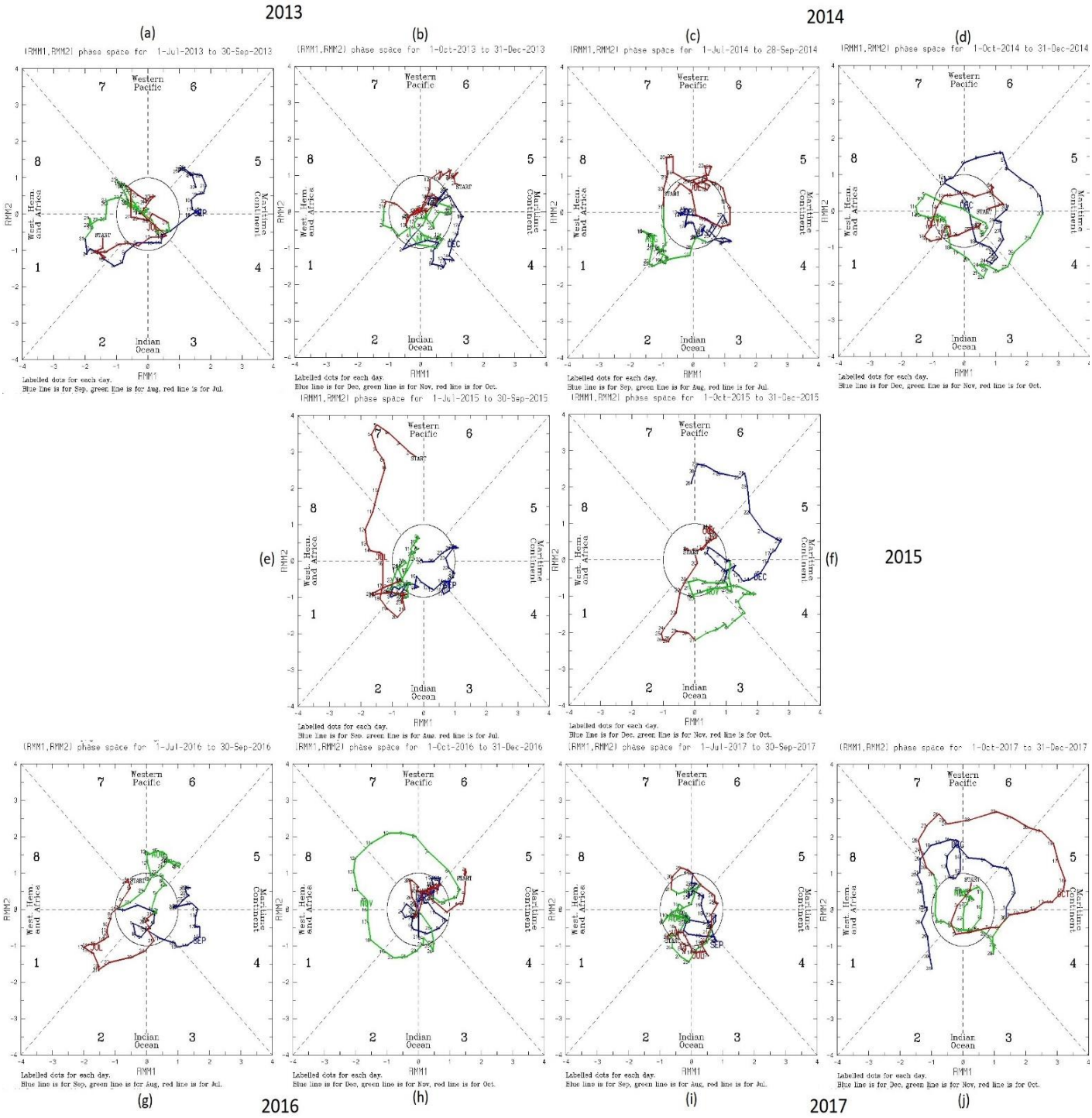

Figure A3: MJO phases (2013-2017) of six months (July-December) in two stages (July-September) in a, c, e, g, i and (October-December) in b, d, f, h, j shown using RMM1 and RMM2 (Real-time Multivariate MJO) method [28] from 2013 till 2017 [29]. Each month in the phase diagram representation starts with red, continues the next month with green and ends with blue line. Inner circle in each phase diagram represents the weakest intensity of MJO. As the MJO line goes far from the inner circle, the intensity increases.

Preprints (www.preprints.org) | NOT PEER-REVIEWED | Posted: 19 June 2018 doi:10.20944/preprints201806.0304.v1

Peer-reviewed version available at Atmosphere 2018, 9, 352; doi:10.3390/atmos9090352

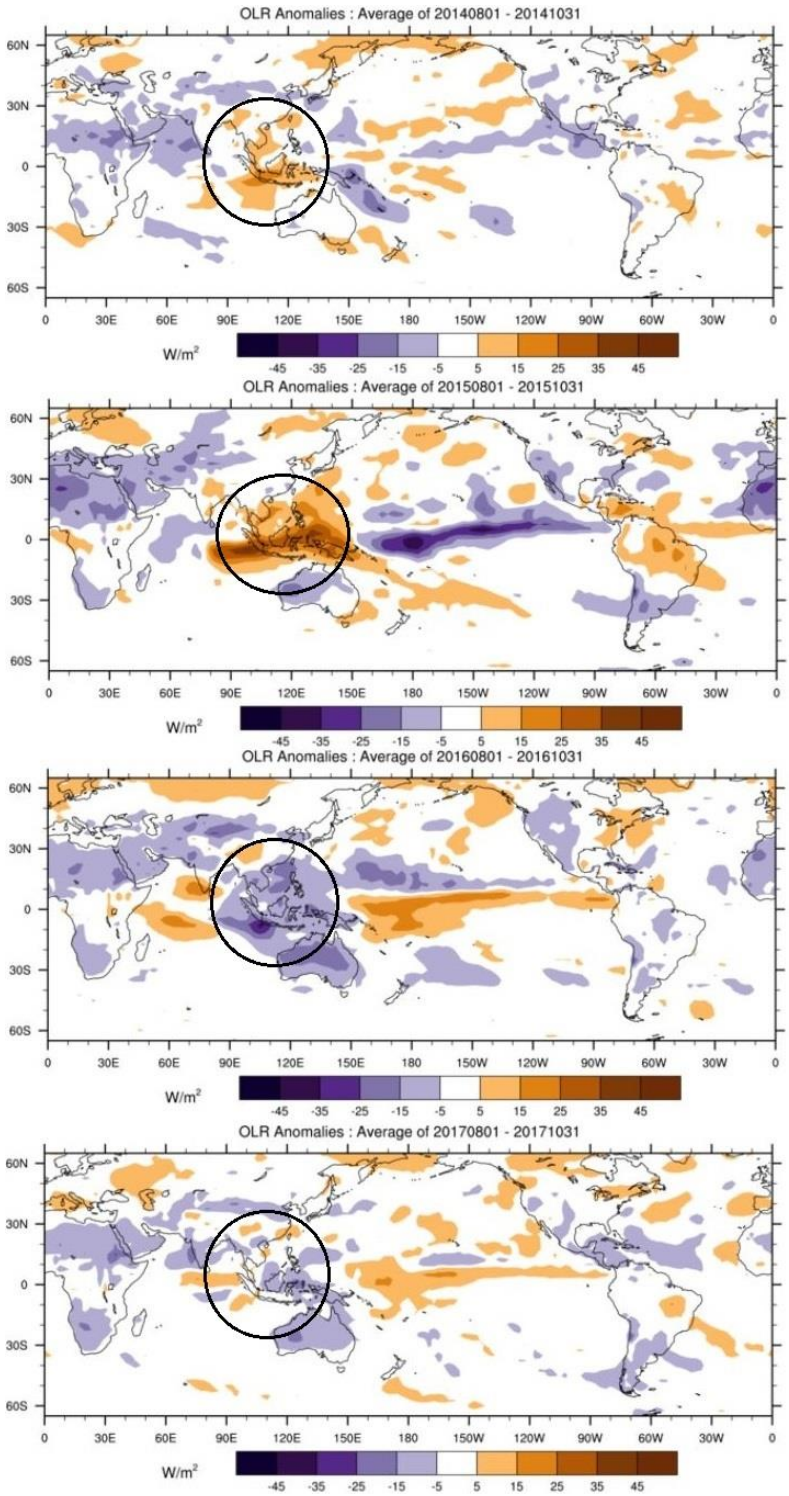

Figure A4 (a): Outgoing longwave radiation (OLR), Wm^{-2} anomalies from 2014 till 2017 (August-October) [31]. Blue shading indicates cloudiness above normal and brown shading indicates cloudiness below normal. Circled part is the area of the study which shows that AUG-OCT of 2015 was the driest period which accordingly was also the peak of BB of the year.

Preprints (www.preprints.org) | NOT PEER-REVIEWED | Posted: 19 June 2018 doi:10.20944/preprints201806.0304.v1

Peer-reviewed version available at Atmosphere 2018, 9, 352; doi:10.3390/atmos9090352

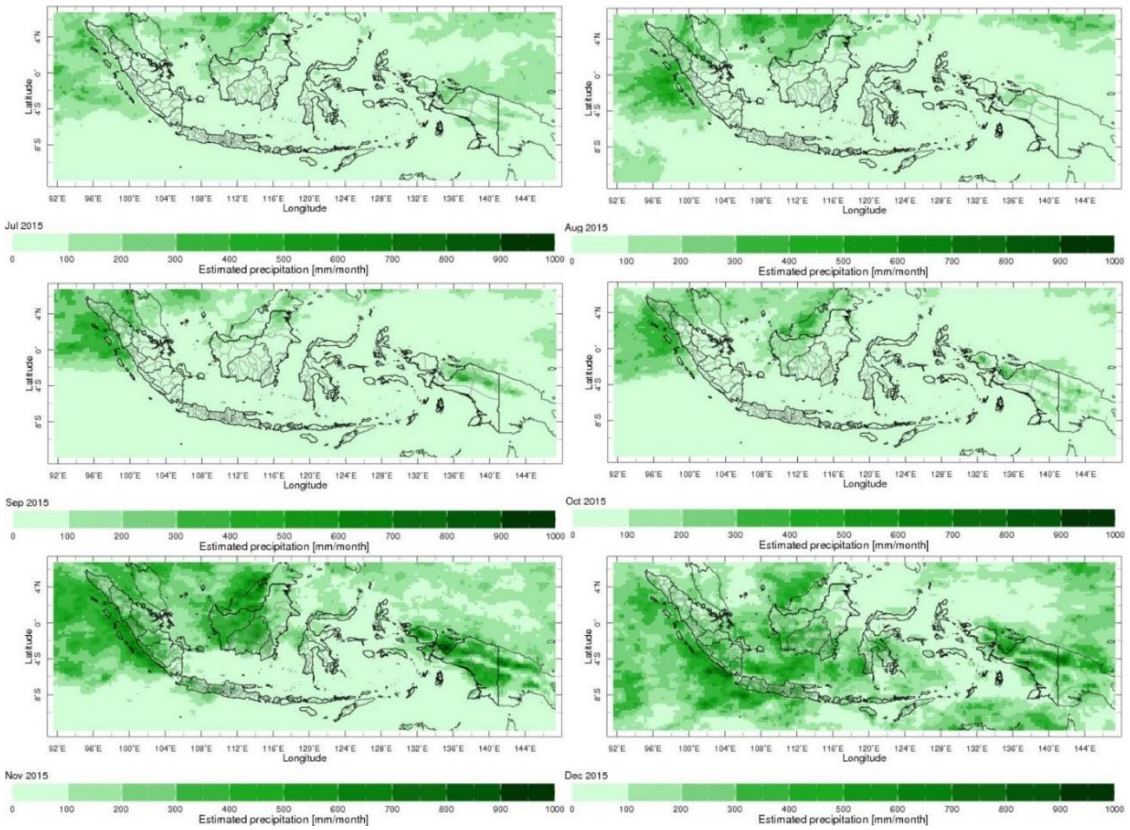

Figure A4 (b): Monthly rainfall analysis data (mm/month) in MC [33]. Figure shows rainfall data from July 2015 till December 2015. Light green shows below normal and dark green shows the above normal respectively. It is seen that during the BB period (AUG-OCT) in the affected area (Malaysia, Sumatra and Kalimantan) precipitation was extremely low which provoked the intensification of burning.

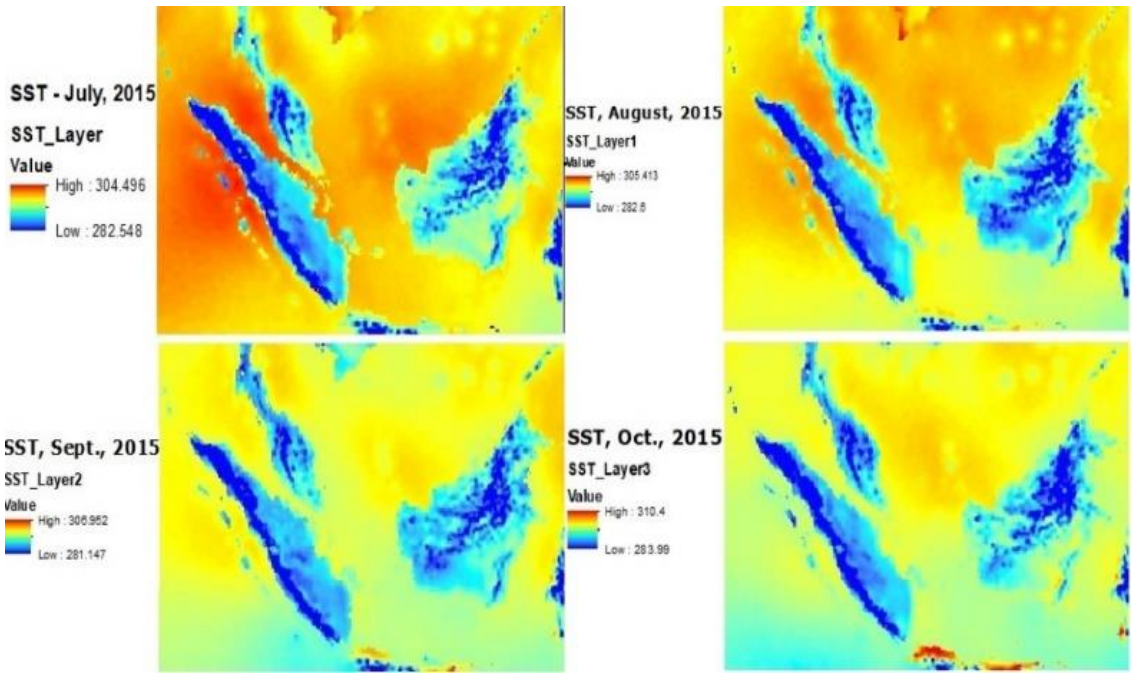

Figure A5: Mean sea surface temperature (SST) for July-October 2015. Figure shows Malaysia, Sumatra and Kalimantan region and SST of their surrounding area during BB of 2015. The SST went up as high as 310.4 K (37.25°C) covered by dark orange shade and as low as low as 303.48 K (30.33 °C) covered by yellow shade. The temperature range was above normal during the BB episode.

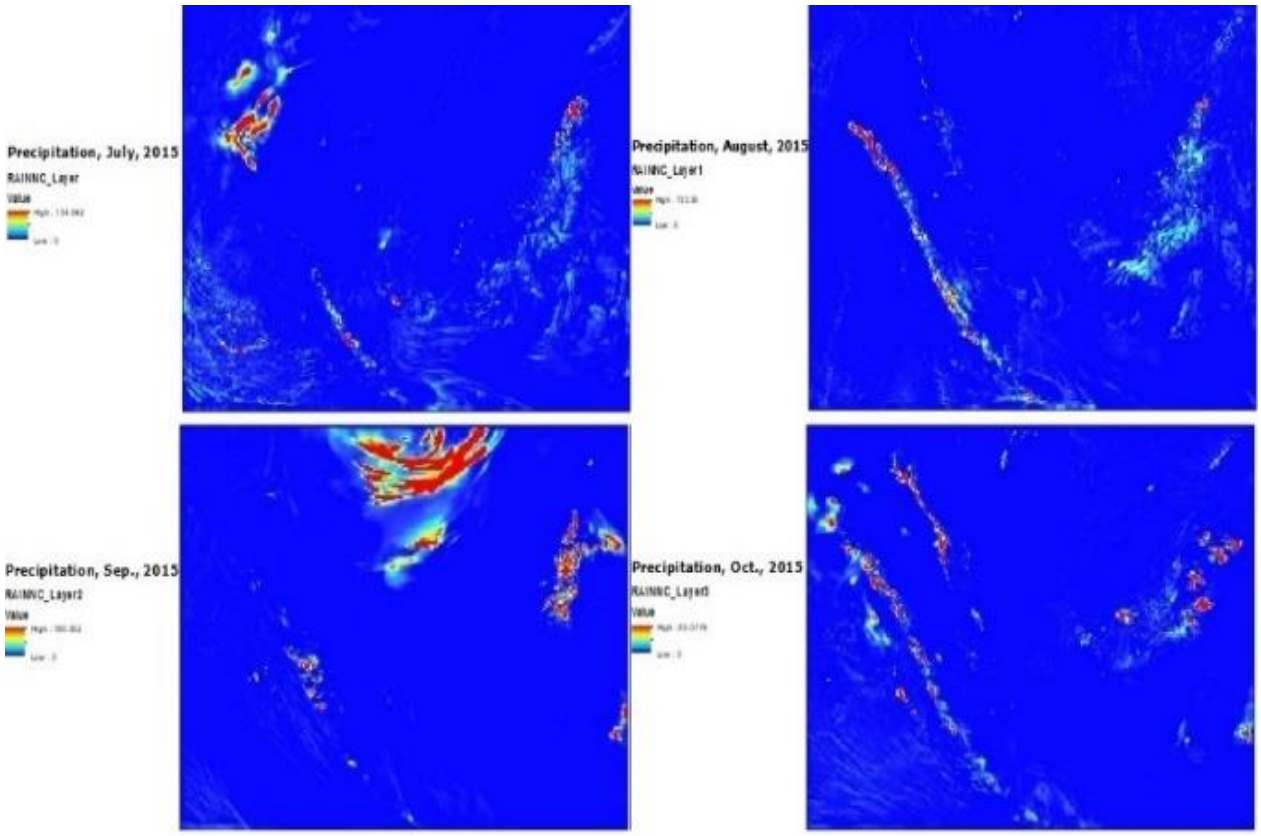

Figure A6: Simulated precipitation rate (rainfall) in Sumatra, Kalimantan and Malaysia region. It shows rainfall data from July to October 2015. Dark blue indicates extremely low rainfall which was less than 3 mm (see Table A2(b)) during 2015 BB episode.

Reference

1. Ramage C. S. (1968). Role of a tropical maritime continent in the atmospheric circulation 1. *Monthly Weather Review*,vol.96 pp.365-370. doi:10.1175/1520-0493(1968)096<0365:ROATMC>2.0.CO;2
2. Richard N. and Jilia S. (2003). The Maritime Continent and Its Role in the Global Climate: A GCM Study. *Journal of Climate, 16*, pp.834-848. doi:10.1175/1520-0442(2003)016<0834:TMCAIR>2.0.CO;2
3. C. P. Chang and Zhuo Wang (2005). Annual Cycle of Southeast Asia - Maritime Continent Rainfall and the Asymmetric Monsoon Transition. *Journal of Climate, 18(2)*, pp.287-301. doi:10.1175/JCLI-3257.1
4. Qian Jian Hua (2008). Why Precipitation Is Mostly Concentrated over Islands in the Maritime Continent. *Journal of the Atmospheric Sciences, 67(11)*, pp.3509–3524. doi:10.1175/2007JAS2422.1
5. Pike, A. C. (1971). Intertropical convergence zone studied with an interacting atmosphere and ocean model. *Monthly Weather Review* , 469-477. Retrieved from http://citeseerx.ist.psu.edu/viewdoc/download?doi=10.1.1.408.6565&rep=rep1&type=pdf
6. Gianotti, L. Rebecca (2012). Assessment of the Regional Climate Model Version 3 over the Maritime Continent Using Different Cumulus Parameterization and Land Surface Schemes. *Journal of Climate, 25*, pp.638-656. doi:10.1175/JCLI-D-11-00025.1
7. Edvin Aldrian and R. Dwi Susanto (2003). Identification of three dominant rainfall regions within Indonesia and their relationship to sea surface temperature. *International Journal of Climatology, 23*(12), pp.1435-1452. doi:10.1002/joc.950
8. P. Rakhmat, As-Syakur, A. Rahman and O. Takahiro (2013). Validation of TRMM Precipitation Radar satellite data over Indonesian region. *Theoretical and Applied Climatology, 12*(3-4), pp.575-587. doi:10.1007/s00704-012-0756-1
9. Zhong, Liu (2012). Tropical Rainfall Measuring Mission (TRMM) Precipitation Data and Services for Research and Applications. *Bulletin of the American Meteorological Society*, pp.1317-1325. doi:10.1175/BAMS-D-11-00152.1

10. A. Giannini, A. W. Robertson and J. H. Qian (2007). A role for tropical tropospheric temperature adjustment to El-Niño Southern Oscillation in the seasonality of monsoonal Indonesia precipitation predictability. *Journal of Geophysical Research: Atmospheres, 112* (D16110), pp.1-14. doi:10.1029/2007JD008519
11. Andreae, P. J. and Crutzen M. O. (1990). Biomass burning in the tropics: impact on atmospheric chemistry and biogeochemical cycles. *Science, 250* (4988), pp.1669-1678. doi:10.1126/science.250.4988.1669
12. G. R. van der Werf, J. T. Randerson, L. Giglio, G. J. Collatz, M. Mu, P. S. Kasibhatla, D. C. Morton, R. S. DeFries, Y. Jin, and T. T. van (2010). Global fire emissions and the contribution of deforestation, savanna, forest, agricultural, and peat fires (1997–2009). *Atmospheric Chemistry and Physics, 10*, pp.11707–11735. doi:10.5194/acp-10-11707-2010
13. Robert D. Field, Guido R. ven der werf, Thierry Fanin, Eric J. Fetzer, Ryan Fuller, Hiren Jethva, Robert Levy, Nathaniel J. Livesey, Ming Luo, Omar Torres and Helen M. Worden (2016, June 21). Indonesian fire activity and smoke pollution in 2015 show persistent nonlinear sensitivity to El-Niño induced drought. *Proceedings of the National Academy of Sciences (PNAS), USA*, pp.1-6. doi:10.1073/pnas.1524888113
14. Md Saidul Islam, Yap Hui Pei and Shrutika Mangharam (2016). Trans-Boundary Haze Pollution in Southeast Asia: Sustainability through Plural Environmental Governance. *Sustainability, 8*(499), pp.1-13. doi:10.3390/su8050499
15. Okimori Y., Ogawa M. & Takahashi F. (2003). Potential of Co2 emission reductions by carbonizing biomass waste from industrial tree plantation in South Sumatra, Indonesia. *Mitigation and Adaptation Strategies for Global Change, 8*(263), pp.261-280. doi:10.1023/B:MITI.0000005643.79908.5a
16. Robert D. Field and Samuel S. P. Shen (2008). Predictability of carbon emissions from biomass burning in Indonesia from 1997 to 2006. *Journal of Geophysical Research , 113*, pp.1-17. doi:10.1029/2008JG000694
17. Jianmin Chen, Chunlin Li, Zoran Ristovski, Andelija Milic, Yuantong Gu, Mohammad S. Islam, Shuxiao Wang, Jiming Hao, Hefeng Zhang, Congrong He, Hai Guo, Hongbo Fu, Branka Miljevic, Lidia Morawska, Phong Thai, Yun Fat Lam, Gavin Pereira and Aijun Ding (2017). A review of biomass burning: Emissions and impacts on air quality, health and climate in China. *Science of The Total Environment, 579*, pp.1000–1034. doi:10.1016/j.scitotenv.2016.11.025
18. Saha K. (2010). *Tropical Circulation Systems and Monsoons.* Berlin, Germany: Springer. doi:10.1007/978-3-642-03373-5
19. Jiang Leishan and Li Tim (2017). Why rainfall response to El Niño over Maritime Continent is weaker and non-uniform in boreal winter than in boreal summer. *Climate Dynamics*, pp.1-19. doi:10.1007/s00382-017-3965-6
20. John L. McBride, Malcolm R. Haylock, and Neville Nicholls (2003). Relationships between the Maritime Continent Heat Source and the El Niño–Southern Oscillation Phenomenon. *Journal of Climate, 16*(17), pp.2905–2914. doi:10.1175/1520-0442(2003)016<2905:RBTMCH>2.0.CO;2
21. Haylock M. and McBride J. (2001). Spatial Coherence and Predictability of Indonesian Wet Season Rainfall. *Journal of Climate, 14*, pp.3882-3887. doi:10.1175/1520-0442(2001)014<3882:SCAPOI>2.0.CO;2
22. Zhang, C. (2013). Madden–Julian Oscillation: Bridging Weather and Climate. *Bulletin of the American Meteorological Society, 94*(12), pp.1849-1870. doi:10.1175/BAMS-D-12-00026.1
23. Ji Hyun Oh, Baek Min Kim, Kwang Yul Kim, Hyo Jong Song and Gyu Ho Lim (2012, June 19). The impact of the diurnal cycle on the MJO over the Maritime Continent: a modeling study assimilating TRMM rain rate into global analysis. *Climate Dynamics, 40*, pp.893–911. doi:10.1007/s00382-012-1419-8
24. A. Mazzarella, A. Giuliacci, and N. Scafetta (2012). Quantifying the Multivariate ENSO Index (MEI) coupling to CO2 concentration and to the length of day variations. *Theoretical Applied Climatology, 111*, pp. 601-607. doi:10.1007/s00704-012-0696-9
25. K. Wolter and M. S. Timlin (1993). *Monitoring ENSO in COADS with a seasonally adjusted principal component index.* University of Oklahoma, School of Meteorology. Norman: Oklahoma Climate Survey. Retrieved from https://www.esrl.noaa.gov/psd/enso/mei/WT1.pdf
26. ESRL/NOAA. (2017, September 12). Dipole Mode Index (DMI). Retrieved May 17, 2018, from Global Climate Observing System (GCOS): https://www.esrl.noaa.gov/psd/gcos_wgsp/Timeseries/Data/dmi.long.data
27. N. H. Saji, and T. Yamagata (2003). Possible impacts of Indian Ocean Dipole mode events on global climate. *Climate Research, 25*(2), pp.151-169. doi:10.3354/cr025151
28. Wheeler M. C. and Harry H. H. (2004, August). An All-Season Real-Time Multivariate MJO Index: Development of an Index for Monitoring and Prediction. *Monthly Weather Review, 132*, pp.1917-1932. doi:10.1175/1520-0493(2004)132<1917:AARMMI>2.0.CO;2

29. Bureau of Meteorology, Australia. (2018, May 17). Madden-Julian Oscillation (MJO). Retrieved from Bureau of Meteorology, Australia: http://www.bom.gov.au/climate/mjo/#tabs=MJO-phase
30. Petty G. W. (2006). *A First Course in Atmospheric Radiation (2nd Ed.) - pp.68.* Madison, Wisconsin: Sundog Publishing.
31. Bureau of Meteorology, Australia. (2018, May 01). Global maps of outgoing longwave radiation (OLR). Melbourne,Victoria, Australia. Retrieved from http://www.bom.gov.au/climate/mjo/#tabs=Cloudiness
32. NASA Earthdata - EOSDIS. *Global Fire Maps*. Retrieved from NASA Worldview:https://worldview.earthdata.nasa.gov/?p=geographic&l=MODIS_Aqua_SurfaceReflectance_Bands143,MODIS_Aqua_SurfaceReflectance_Bands721,MODIS_Terra_SurfaceReflectance_Bands143,MODIS_Terra_SurfaceReflectance_Bands721,VIIRS_SNPP_CorrectedReflectance_TrueColor(hi
33. Joyce R. J., Janowiak J. E. Arkin P. A. and Xie P. (2004, June 01). CMORPH: A Method that Produces Global Precipitation Estimates from Passive Microwave and Infrared Data at High Spatial and Temporal Resolution. *Journal of Hydrometeorology, 05*, pp.487-503. doi:10.1175/1525-7541(2004)005<0487:CAMTPG>2.0.CO;2
34. UCAR NCAR RDA. (2015, July 01). *NCEP GDAS/FNL 0.25 Degree Global Tropospheric Analyses and Forecast Grids*. doi:10.5065/D65Q4T4Z
35. NOAA. (2018, May 17). *Bimonthly MEI values*. Retrieved from Multivariate ENSO Index (MEI): https://www.esrl.noaa.gov/psd/enso/mei/table.html
36. Ashok K. and Guan Z. (2004, August 15). Individual and Combined Influences of ENSO and the Indian Ocean Dipole on the Indian Summer Monsoon. *Journal of Climate*, pp.3141-3155. doi:10.1175/15200442(2004)017<3141:IACIOE>2.0.CO;2
37. Gary Meyers, Peter McIntosh, Lidia Pigot and Mike Pook (2007). The Years of El Niño, La Niña, and interactions with the tropical Indian Ocean. *Journal of Cimate, 20*, pp. 2872-2880. doi:10.1175/JCLI4152.1
38. Zhang, C. (2005, June 30). MADDEN-JULIAN OSCILLATION. *Reviews of Geophysics, 43*(2), 1-36. doi:10.1029/2004RG000158
39. Nathan P. Arnold, Zhiming Kuang and Eli Tziperman (2012). Enhanced MJO-like Variability at High SST. *Journal of Climate* , pp.988-1001. doi:10.1175/JCLI-D-12-00272.1
40. Song-You Hong, Jimy Dudhia and Shu-Hua Chen (2004, January). A Revised Approach to Ice Microphysical Processes for the Bulk Parameterization of Clouds and Precipitation. *Monthly Weather Reveiw*, 103-120. doi:10.1175/1520-0493(2004)132<0103:ARATIM>2.0.CO;2
41. Eli J. Mlawer, Steven J. Taubman, Patrick D. Brown, Michael J. Iacono and Shepard A. Clough (1997). Radiative transfer for inhomogeneous atmospheres: RRTM, a validated correlated-k model for the longwave. *Journal of Geophysical Research, 102*(D14), 16663-16682. doi:10.1029/97JD00237
42. Dudhia, J. (1989). Numerical Study of Convection Observed during the Winter Monsoon Experiment Using a Mesoscale Two-Dimensional Model. *Journal of the Atmospheric Sciences*, 3077-3107. doi:10.1175/1520-0469(1989)046<3077:NSOCOD>2.0.CO;2
43. Monin A.S and Obukhov A.F.M. (1954). Basic laws of turbulent mixing in the surface layer of the atmosphere. *Contrib. Geophys. Inst. Acad. Sci. USSR, 24*(151), 163-187. Retrieved from http://www2.mmm.ucar.edu/wrf/users/phys_refs/SURFACE_LAYER/eta_part1.pdf
44. Guo-Yue Niu, Zong-Liang Yang, Kenneth E. Mitchell, Fei Chen, Michael B. Ek, Michael Barlage, Anil Kumar, Kevin Manning, Dev Niyogi, Enrique Rosero, Mukul Tewari and Youlong Xia (2011). The community Noah land surface model with multiparameterization options (Noah-MP): 1. Model description and evaluation with local-scale measurements. *Journal of Geophysical Research , 116*(D12109), 1-19. doi:10.1029/2010JD015139
45. Hong, Song–You, Yign Noh, Jimy Dudhia, 2006: A new vertical diffusion package with an explicit treatment of entrainment processes. Mon. Wea. Rev., 134, 2318–2341. doi: 10.1175/MWR3199.1

46. Kain, J. S. (2004). The Kain–Fritsch Convective Parameterization: An Update. *Journal of Applied Meteorology*, *43*, 170-181. doi:10.1175/1520-0450(2004)043<0170:TKCPAU>2.0.CO;2

47. Global Climate Observing System (GCOS). (2017, September 12). DMI: Standard PSD Format. Boulder, Colorado, USA. Retrieved from https://www.esrl.noaa.gov/psd/gcos_wgsp/Timeseries/Data/dmi.long.data